Mathematical Medicine and Biology (2014) **31**, 365–392
doi:10.1093/imammb/dqt004
Advance Access publication on August 18, 2013

Patient-specific modelling of head-up tilt

Nakeya D. Williams
Department of Mathematics, North Carolina State University, Raleigh, NC 27695, USA

Øistein Wind-Willassen
Department of Science, Systems and Models, Roskilde University, 4000 Roskilde, Denmark

Andrew A. Wright and REU Program[†]
Department of Mathematics, North Carolina State University, Raleigh, NC 27695, USA

Jesper Mehlsen
Coordinating Research Centre, Frederiksberg Hospital, 2000 Frederiksberg, Denmark.

Johnny T. Ottesen
Department of Science, Systems and Models, Roskilde University, 4000 Roskilde, Denmark

and

Mette S. Olufsen[*]
Department of Mathematics, North Carolina State University, Raleigh, NC 27695, USA
[*]Corresponding author: Email: msolufse@ncsu.edu

[Received on 6 June 2012; revised on 4 January 2013; accepted on 21 February 2013]

Short-term cardiovascular responses to head-up tilt (HUT) involve complex cardiovascular regulation in order to maintain blood pressure at homoeostatic levels. This manuscript presents a patient-specific model that uses heart rate as an input to fit the dynamic changes in arterial blood pressure data during HUT. The model contains five compartments representing arteries and veins in the upper and lower body of the systemic circulation, as well as the left ventricle facilitating pumping of the heart. A physiologically based submodel describes gravitational pooling of the blood into the lower extremities during HUT, and a cardiovascular regulation model adjusts cardiac contractility and vascular resistance to the blood pressure changes. Nominal parameter values are computed from patient-specific data and literature estimates. The model is rendered patient specific via the use of parameter estimation techniques. This process involves sensitivity analysis, prediction of a subset of identifiable parameters, and non-linear optimization. The approach proposed here was applied to the analysis of aortic and carotid HUT data from five healthy young subjects. Results showed that it is possible to identify a subset of model parameters that can be estimated allowing the model to fit changes in arterial blood pressure observed at the level of the carotid bifurcation. Moreover, the model estimates physiologically reasonable values for arterial and venous blood pressures, blood volumes and cardiac output for which data are not available.

Keywords: cardiovascular system dynamics; head-up tilt; sensitivity analysis; subset selection; parameter estimation.

[†]REU Program: B.C. Stitchnot, Murray State University; J. Cuffie, Albany State University; C. Sabett, St. Mary's College; A. Brown, Spelman College; A. Soto, Cal Poly Ponoma; O. Lu, Zhejiang University, China.

1. Introduction

The head-up tilt (HUT) test is often used to assess a patient's ability to regulate blood pressure (Miller & Kruse, 2005; Lanier *et al.*, 2011), in particular for patients suffering from frequent episodes of syncope, lightheadedness or dizziness (Miller & Kruse, 2005). During this procedure quantities measured include non-invasive beat-to-beat recordings of arterial blood pressure and heart rate. The test starts with the patient placed on a tilt-table in the supine position. After steady values for pressure and heart rate are obtained the table is tilted to an angle of 60–70°. Upon tilting, gravity causes pooling of 500–1000 ml of blood in the lower extremities reducing the venous return, cardiac filling and cardiac output (Rowell *et al.*, 2004; Lanier *et al.*, 2011). The change of volume leads to a decrease in blood pressure in the upper body (above the centre of gravity), while blood pressure in the lower body (below the centre of gravity) is increased. During HUT the baroreceptors located in the carotid sinus sense the drop in blood pressure causing sympathetic activation and parasympathetic withdrawal. This in turn leads to an increase in heart rate, along with changes in cardiac contractility and vascular resistance (Tortora & Anagnostakos, 1990; Guyton & Hall, 1996; Robertson *et al.*, 2004). For most people, the receptors located in the aortic arch sense an increase in pressure (Enishi *et al.*, 2004; Lanier *et al.*, 2011), which in principle should cause a decrease in heart rate. This response is contradictory to observed heart rate increase. Thus, we hypothesize that during HUT, the carotid sinus baroreceptors are the main receptors activated leading to the observed increase in heart rate. Consequently, models developed to analyse the dynamics of blood pressure regulation were compared with data measured at the level of the carotid sinus. However, in most tilt-table experiments blood pressure is measured at the level of the aortic arch. In this study, we use data from both locations. Figure 1a shows an example of blood pressure time-series measured at

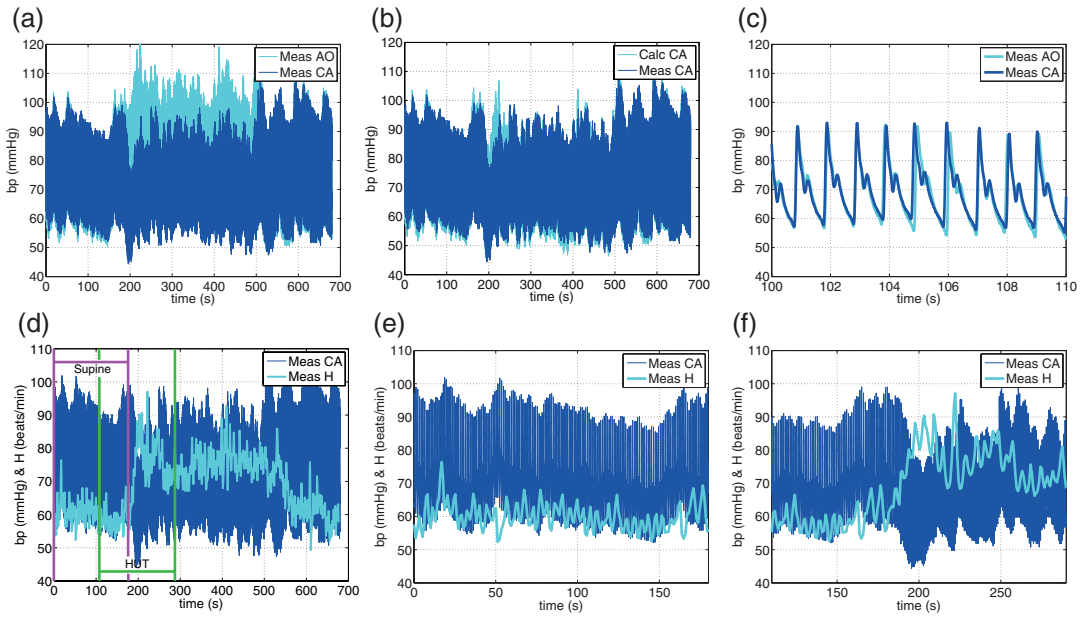

FIG. 1. (a) Simultaneous measurements of aortic (cyan) and carotid (blue) blood pressures during HUT, (b) measured (blue) and calculated (cyan) carotid blood pressure and (c) a zoom for $t = 100$–110 s. (d–f) Measured carotid blood pressure (blue) and heart rate (cyan) for the complete dataset (d), for data used to estimate the dynamics in the supine position (e) (marked with pink lines on (d)), and during HUT (f) (marked with green lines on (d)). Note that there is an overlap between the data shown in (e) and (f).

the two locations. Data measured at the level of the carotid sinus are used directly, while data measured at the level of the aortic arch are first translated to the level of the carotid sinus. Figure 1b shows an example of measured and calculated carotid blood pressures.

The baroreflex system, described above, is the main contributor to the control engaged during HUT. However, other sensory systems also play a role in modulating the vascular targets including inputs from cardiopulmonary sensors, the vestibular system, the central command centre and the muscle sympathetic system (Abboud *et al.*, 1979; Ogoh *et al.*, 2006). In this study, we do not directly model the afferents but focus on predicting the impact on the vascular targets: heart rate, cardiac contractility, and vascular resistance by allowing model parameters, representing these quantities to vary in time. The time-varying parameters are embedded in a compartmental model including the left heart as well as arterial and venous compartments representing the upper (above the centre of gravity) and lower (below the centre of gravity) parts of the body. Heart rate and the time for end-systole are used as the model inputs, whereas systolic and diastolic arterial blood pressures in the upper body (representing pressure at the level of the carotid arteries) are the model outputs. Parameter estimation techniques are used to render the model patient-specific allowing the model to fit blood pressure dynamics observed at the level of the carotid arteries.

The paper is organized as follows: The methods are outlined in Section 2. This section includes a description of the data (Section 2.1); the cardiovascular model, and methods used for the calculation of nominal parameter values and initial conditions (Section 2.2); model analysis including a formulation of the optimization problem, sensitivity analysis, parameter identification and methods used for non-linear optimization (Section 2.3). Results are presented in Section 3, and we conclude with Section 4 discussing our findings.

2. Methods

A large number of previous studies have analysed cardiovascular regulation of heart rate from a medical, statistical and modelling point of view. These studies can be separated in two groups: studies which analyse the system dynamics using signal processing techniques and studies that are based on mechanistic differential equations models. Signal processing-based studies (e.g. Seidel *et al.*, 1997; Eckberg, 2008; Chen *et al.*, 2010; Porta *et al.*, 2012) typically analyse the frequency and magnitude components of the measured signals. Mechanistic models investigate the system dynamics using techniques developed from physical laws. Such models are often used to describe dynamics for an average healthy subject, or to predict the impact of a given disease (e.g. Guyton *et al.*, 1972; Rideout, 1991; Melchior *et al.*, 1992; Bauernschmitt *et al.*, 1999; Le Vey & Vermeiren, 2000; Olansen *et al.*, 2000; Ottesen, 2000; Olufsen *et al.*, 2002; van Heusden *et al.*, 2006; Sheffer *et al.*, 2007; Silvani *et al.*, 2011). While the signal processing techniques typically analyse actual signals from individual subjects, mechanistic models are most commonly developed to gain more insight into the system, i.e. they were not adapted to display individual dynamics. Patient-specific models, which use mechanistic descriptions to predict signals recorded from individual subjects, can be obtained by combining a general mechanistic model with patient-specific estimation of model parameters. Estimating model parameters involve solution of an inverse problem, i.e. given a model and data one has to estimate the model parameters (Banks *et al.*, 2009). This problem is in general difficult to solve, and typically, no unique analytical or numerical solution can be found (Zenker *et al.*, 2009).

One of the main obstacles in developing patient-specific models is that ‘good’ physiologically models often have a large number of variables and parameters, while the number of quantities measured to render these models patient specific is sparse. Therefore, most studies addressing parameter

identification and/or parameter estimation use examples involving a 'correct' model, good initial parameter values and a comprehensive set of data. For such systems, model parameters may be estimated via solution of the associated inverse problem (Cintron-Arias *et al.*, 2009). However, in practice, only some parameters can be estimated given a model and available observations, and this process works better if the model analysed is not too complex.

The overall objective should be to build a simple model including only essential elements. Some studies have successfully developed patient-specific models of the cardiovascular system, but most of these models do not include pulsatility (Batzel *et al.*, 1999; Fink *et al.*, 2004; van de Vooren *et al.*, 2007). We have developed a few models that include pulsatility (Olufsen *et al.*, 2005; Pope *et al.*, 2009), though the model by Olufsen *et al.* (2005) estimated too many model parameters and the model by Pope *et al.* (2009) only addressed how to estimate parameters for a subject in the supine position. Other contributions include the study by TenVoorde & Kingma (2000) who developed a model predicting short-term blood pressure and heart rate variability for a healthy young male, and studies by Ursino who modelled heart rate regulation (Ursino, 1998, 1999; Silvani *et al.*, 2011). The latter studies did compare the model output with experimental data, but did not address parameter estimation. Another example, is the recent model by Bugenhagen *et al.* (2010), which computes heart rate regulation in rats. This study does address parameter estimation, but does not address parameter identifiability.

The study presented here builds on these previous efforts. We have built a simple model that uses heart rate as input and estimates pulsatile arterial blood pressure during HUT. To make the model patient specific, we use sensitivity analysis and parameter identification combined with non-linear optimization. The study shows how to estimate constant and time-varying parameters allowing the model-fit data measured at the level of the carotid artery. Finally, we show how carotid pressure can be calculated from data measured at the level of the aorta and that similar parameter estimates are obtained comparing model outputs against the measured and calculated carotid pressures.

2.1 *Blood pressure and heart rate data*

Data were collected at the Coordinating Research Centre at Frederiksberg Hospital, Copenhagen, Denmark from five healthy young male volunteers age 30 ± 4 who were fit and had no known heart or vascular diseases. The subjects gave informed consent to participate in the study, which was approved by the local internal review board at Frederiksberg Hospital, Denmark. After resting for 10 min in the supine position, the subjects were tilted to an angle of 60° at a speed of 15°/s measured by way of an electronic marker. The subjects remained tilted for 5 min, and were then returned to the supine position at the same tilt speed. For the model-based analysis, we extracted a total of 290 s of data: including a 180 s segment recorded while the subjects were in the supine position (see Fig. 1e) and a 180 s segment recorded during HUT (see Fig. 1f). This latter segment overlaps with the supine segment as illustrated in the figure.

Measurements include ECG recorded using standard precordial leads and blood pressure recorded using photoplethysmography (Finapres Medical Systems B.V.). For pressure measurements, a sensor was placed on the index finger on each hand. The left hand was kept at the level of the aortic arch, which is at the same level as the mitral valve, whereas the right hand was kept at the level of the carotid sinus, which is at the same level as the carotid bifurcation. The location of the mitral valve and carotid bifurcation were determined by echocardiography and carotid ultrasound, respectively. ECG and blood pressure measurements were sampled continuously at a rate of 1.0 kHz and saved digitally using an A/D-converter communicating with a computer via Chart 5 (ADInstruments). This program allows extraction of heart rate from the ECG measurement. By keeping the fingers with sensors at the two

locations, the measured pressures hydrostatically represents the actual pressures at the two locations. Diastolic values measured are similar to the central pressure values, though systolic values may be overestimated due to the impact of wave reflection. Examples of peripheral and central wave forms can be found in the book by Fung (1996). Figure 1a–c shows the two blood pressure time series for a representative subject, whereas Fig. 1d–f shows heart rate and blood pressure time series measured at the level of the carotid arteries.

As discussed in the introduction, to estimate the blood pressure regulation in response to HUT, blood pressure should be measured at the level of the carotid sinus. However, many existing tilt experiments have only measured blood pressure at the level of the aorta. For an upright subject, the main difference between the two signals is the impact of hydrostatic pressure. Thus, using a simple model involving gravity, it is possible to calculate the carotid pressure $p_{Ca,p}$ from the pressure measured at the level of the aortic arch as

$$p_{Ca,p} = p_{Ao} - \rho g h, \tag{2.1}$$

where p_{Ao} is the measured aortic blood pressure data, ρ (g/ml) is the density of blood, g (cm/s^2) is the constant of gravitational acceleration, and h (cm) is the height difference between the carotid sinus and the aortic arch. Figure 1b shows the true carotid data along with the calculated carotid data.

2.2 *Mathematical model*

This section describes the cardiovascular model developed to estimate the blood flow, volume and pressure in the systemic circulation during HUT. The model development is split into three parts including development of: a lumped cardiovascular model estimating dynamics while the subject is in the supine position; a model estimating dynamic changes in response to HUT and a model estimating the impact of cardiovascular regulation on the model parameters. Following the model descriptions, we include a section describing nominal parameter values and initial conditions used to solve the differential equations.

2.2.1 *Lumped cardiovascular model.* The basic cardiovascular model includes five compartments (see Fig. 2) representing arteries and veins in the upper and lower body of the systemic circulation, as well as the left heart. The upper body compartments include arteries and veins in the head, thorax and abdomen, whereas the lower body compartments include all vessels in the legs. The model mimics an electrical RC-circuit with voltage analogous to pressure, current analogous to flow, charge analogous to volume and compliance analogous to capacitance, while resistance is the same in both formulations. This model is able to estimate pulsatile blood pressure and flow in the various compartments, while it cannot output the actual shape of the wave form.

For each compartment, a pressure–volume relation can be defined as

$$V_i - V_{\text{un}} = C_i(p_i - p_{\text{ext}}), \tag{2.2}$$

where V_i (ml) is the compartment volume, V_{un} (ml) is the unstressed volume, C_i (ml/mmHg) is the compartment compliance, p_i (mmHg) is the compartment instantaneous blood pressure and p_{ext} (mmHg) (assumed constant) is the pressure in the surrounding tissue. For each compartment, we also use a differential equation to predict the change in volume,

$$\frac{\mathrm{d}V_i}{\mathrm{d}t} = q_{\text{in}} - q_{\text{out}}, \tag{2.3}$$

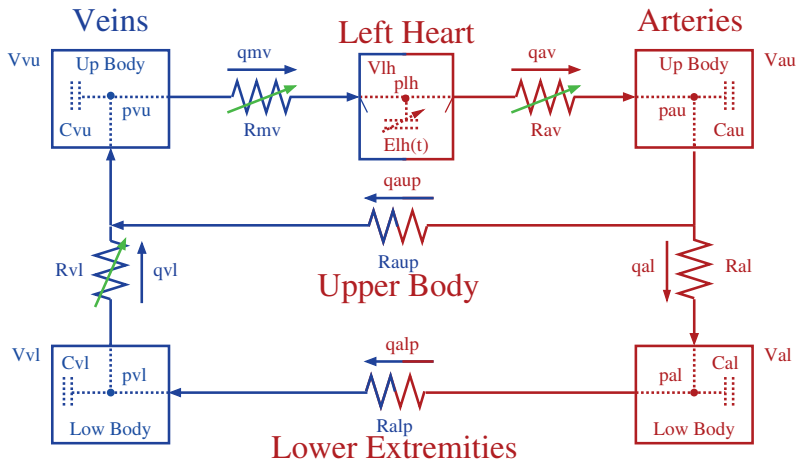

FIG. 2. Compartment model used for predicting HUT dynamics. For each compartment an associated blood pressure p (mmHg), volume V (ml) and compliance C (ml/mmHg) are defined. The compartments represent the upper body arteries (subscript *au*), lower body arteries (subscript *al*), upper body veins (subscript *vu*), lower body veins (subscript *vl*) and the left heart (subscript *lh*). Resistances R (mmHg s/ml) are placed between all compartments: R_{al} denotes the resistance between arteries in the upper and lower body; R_{aup} and R_{alp} denote the resistance between arteries and veins in the upper and lower body, respectively. The two heart valves, the mitral valve and the aortic valve, are modelled as pressure-dependent resistors R_{mv} and R_{av}. Finally, the resistance between the lower and upper body veins R_{vl} is also modelled as pressure dependent to prevent the retrograde flow into the lower-body during the HUT.

where q (ml/s) is the volumetric flow. Using a linear relationship analogous to Ohm's law, the volumetric flow q (ml/s) between compartments can be computed as

$$q = \frac{p_{\text{in}} - p_{\text{out}}}{R}, \tag{2.4}$$

where p_{in} and p_{out} are the pressure on either side of the resistor R (mmHg s/ml). Differentiating (2.2), using (2.3), and inserting (2.4) allows us to obtain a system of differential equations in blood pressure of the form

$$\frac{\mathrm{d}p_i}{\mathrm{d}t} = \frac{1}{C_i}\frac{\mathrm{d}V_i}{\mathrm{d}t} = \frac{1}{C_i}\left(\frac{p_{i-1} - p_i}{R_{i-1}} - \frac{p_i - p_{i+1}}{R_i}\right),$$

where i refers to the compartment for which the pressure p_i is computed, while $i-1$ and $i+1$ refer to the two neighbouring compartments. For resistances that appear between compartments, R_{i-1} refers to the resistance between compartments $i-1$ and i, and R_i refers to the resistance between compartments i and $i+1$. The latter equation is valid since we assume that C_i (ml/mmHg) is constant. This formulation is utilized for the four arterial and venous compartments.

For the left heart compartment, we also use (2.3). For this compartment, pressure is predicted from volume using the pressure–volume relation

$$p_{\text{lh}} = E_{\text{lh}}(V_{\text{lh}} - V_{\text{un}}), \tag{2.5}$$

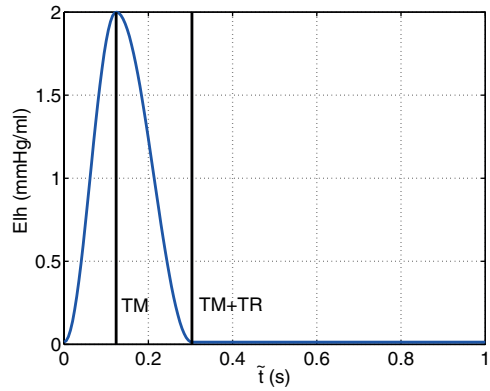

FIG. 3. Time-varying elastance during a cardiac cycle. The maximum elastance is found at $\tilde{t} = T_M$ and the minimal elastance at $\tilde{t} = T_M + T_R$, while the length of the cardiac cycle $T = 1$ s. Values for T_M and $T = 1/H$ are obtained from data.

where E_{lh} (mmHg/ml) is the left heart elastance (the reciprocal of its compliance) and V_{lh} is the left heart volume. Pumping is achieved by introducing a variable elastance function (Ellwein, 2008) of the form

$$E_{\text{lh}}(\tilde{t}) = \begin{cases} \dfrac{E_{\max} - E_{\min}}{2}\left[1 - \cos\left(\dfrac{\pi\tilde{t}}{T_M}\right)\right] + E_{\min} & 0 \leqslant \tilde{t} \leqslant T_M \\ \dfrac{E_{\max} - E_{\min}}{2}\left[\cos\left(\dfrac{\pi\left(\tilde{t} - T_M\right)}{T_R}\right) + 1\right] + E_{\min} & T_M \leqslant \tilde{t} \leqslant T_M + T_R \\ E_{\min} & T_M + T_R \leqslant \tilde{t} \leqslant T \end{cases}, \tag{2.6}$$

where $\tilde{t}$ is the time within a cardiac cycle $T = 1/H$. Here, $E_{\min}$ and $E_{\max}$ denote the minimum and maximum elastance, respectively. For each cardiac cycle elastance is increased for $0 < \tilde{t} < T_M$ and decreased for $T_M < \tilde{t} < T_M + T_R$, while during diastole $T_M + T_R < \tilde{t} < T$ elastance is kept constant at its minimum value. Values for T and T_M are obtained from data, whereas T_R is a model parameter. The time-varying elastance function is illustrated in Fig. 3.

Finally, heart valves are modelled using pressure-dependent resistors for which a large resistance R_{cl} represents a closed valve, whereas a small resistance R_{op} represents an open valve. These are modelled as smooth sigmoidal functions of the form

$$R_v = R_{\text{cl}} - \frac{R_{\text{cl}} - R_{\text{op}}}{1 + \mathrm{e}^{-\beta(p_{\text{in}} - p_{\text{out}})}}, \tag{2.7}$$

where p_{in} and p_{out} denote the pressures in compartments on either side of the valve. For $p_{\text{in}} > p_{\text{out}}$, $R_v \to R_{\text{op}}$ (the valve is open), and when $p_{\text{out}} > p_{\text{in}}$, the valve closes.

Using these relations the five differential equations can be written as

$$\frac{\mathrm{d}p_{\text{au}}}{\mathrm{d}t} = (q_{\text{av}} - q_{\text{al}} - q_{\text{aup}})/C_{\text{au}},$$
$$\frac{\mathrm{d}p_{\text{al}}}{\mathrm{d}t} = (q_{\text{al}} - q_{\text{alp}})/C_{\text{al}},$$

TABLE 1 *Abbreviations (subscripts) used in the compartmental model*

Abbreviation	Name
av	Aortic valve
au	Upper body arteries
al	Lower body arteries
aup	Upper body 'peripheral' vascular bed
alp	Lower body 'peripheral' vascular bed
vu	Upper body veins
vl	Lower body veins
lh	The left heart (ventricle and atrium)

$$\frac{\mathrm{d}p_{\mathrm{vl}}}{\mathrm{d}t} = (q_{\mathrm{alp}} - q_{\mathrm{vl}})/C_{\mathrm{vl}},$$
$$\frac{\mathrm{d}p_{\mathrm{vu}}}{\mathrm{d}t} = (q_{\mathrm{aup}} + q_{\mathrm{vl}} - q_{\mathrm{mv}})/C_{\mathrm{vu}},$$
$$\frac{\mathrm{d}V_{\mathrm{lh}}}{\mathrm{d}t} = q_{\mathrm{mv}} - q_{\mathrm{av}},$$

where

$$q_{\mathrm{av}} = \frac{p_{\mathrm{lh}} - p_{\mathrm{au}}}{R_{\mathrm{av}}},$$
$$q_{\mathrm{aup}} = \frac{p_{\mathrm{au}} - p_{\mathrm{vu}}}{R_{\mathrm{aup}}},$$
$$q_{\mathrm{al}} = \frac{p_{\mathrm{au}} - p_{\mathrm{al}}}{R_{\mathrm{al}}},$$
$$q_{\mathrm{alp}} = \frac{p_{\mathrm{al}} - p_{\mathrm{vl}}}{R_{\mathrm{alp}}},$$
$$q_{\mathrm{vl}} = \frac{p_{\mathrm{vl}} - p_{\mathrm{vu}}}{R_{\mathrm{vl}}},$$
$$q_{\mathrm{mv}} = \frac{p_{\mathrm{vu}} - p_{\mathrm{lh}}}{R_{\mathrm{mv}}}.$$

In the last set of equations, the left ventricular pressure (p_{lh}) is predicted using (2.5), the pressure-dependent resistances used to model the valves ($R_{\mathrm{av}}, R_{\mathrm{mv}}$) are predicted from (2.7) and the total blood volume can be computed from pressures using (2.2). These equations were solved in Matlab using the ODE15s differential equations solver. Abbreviations (subscripts) are given in Table 1.

2.2.2 *Modelling HUT.* The response to HUT is modelled by accounting for hydrostatic pressure acting on each compartment. During the supine position, gravity does not influence the system. Upon HUT, blood is pooled in the lower extremities leading to an increase in pressure in the lower body, while pressure in the upper body decreases. To account for gravity, the pressure at the level of the carotid arteries is used as a reference pressure, so an extra term is added to the flow (q_{al}) and subtracted

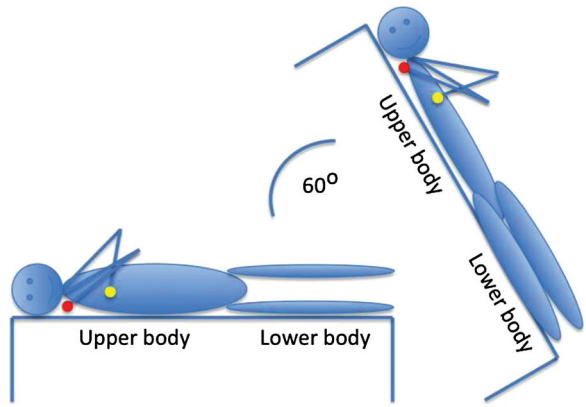

FIG. 4. The HUT test: the subject depicted is tilted to an angle of 60° at a constant speed of 15° /s. Red and yellow circles indicate the locations for the blood pressure sensors. Each sensor is mounted on the index finger, one finger (red) is placed at the level of the carotid artery, while the other (yellow) is placed at the level of the heart. Upon HUT blood is pooled in the lower extremities.

from the flow (q_{vl}) of the lower body compartments. Figure 4 shows the subject tilted at an angle $\theta = 60^\circ$. The quantity h_{tilt} (cm) represents the distance between the lower and upper compartment. The gravitational effects are calculated as in Olufsen *et al.* (2005), and the modified flow equations are given by

$$q = \frac{\rho g h_{\text{tilt}} \sin(\theta(t)) + p_{\text{in}} - p_{\text{out}}}{R},$$
$$\theta(t) = \frac{\pi}{180} \begin{cases} 0 & t < t_{\text{st}} \\ v_t(t - t_{\text{st}}) & t_{\text{st}} \leqslant t \leqslant t_{\text{st}} + t_{\text{ed}} \\ 60 & t > t_{\text{st}} + t_{\text{ed}} \end{cases}, \tag{2.8}$$

where ρ (g/ml) is the blood density, g (cm/s^2) is the constant of gravitational acceleration, h_{tilt} (cm) is the absolute height between the upper body and lower body compartments, $\theta(t)$ is the tilt angle (in radians) and $v_t = 15^\circ$/s is the tilt speed, while t_{st} and t_{ed} denote the time at which HUT is started and ended, respectively. The combined term $\rho g h_{\text{tilt}} \sin(\theta(t))$ denotes the hydrostatic pressure between the upper and lower body compartments.

2.2.3 *Modelling effects of cardiovascular regulation.* Upon HUT firing of the baroreceptor nerves are modulated by the aortic and carotid sinus baroreceptors sensing changes in the stretch of the arterial wall. Typically, HUT leads to a decrease in blood pressure mediating an increase in sympathetic outflow along with parasympathetic withdrawal. Sympathetic stimulation elicits changes in vascular resistance and cardiac contractility, whereas parasympathetic withdrawal primarily has an effect on heart rate (shown on Fig. 1) and cardiac contractility. Heart rate is used as an input, thus the parasympathetic heart rate regulation is implicitly accounted for in the model. Regulation of cardiac contractility is modelled by controlling the minimum elastance of the left heart (E_{min}), while regulation of vascular resistance is included in the upper and lower body. The upper body compartment includes abdominal and intestinal vessels, while the lower body compartment lumps vessels in the lower extremities. Consequently, both

R_{aup} and R_{alp} (see Fig. 2) have been regulated. However, as the compartments representing the upper and lower body arteries appear in parallel, both resistances are not identifiable, thus we control R_{aup} directly, while we let $R_{alp} = kR_{aup}$, where k is the ratio of the optimized supine values of R_{aup} and R_{alp}.

Two quantities were controlled (R_{aup}, E_{min}) to counteract the effect of the tilt. We modelled the control by defining the controlled quantities using piecewise linear functions of time given by

$$X(t) = \sum_{i=1}^{N} \gamma_i H_i(t),$$
$$H_i(t) = \begin{cases} \dfrac{t - t_{i-1}}{t_i - t_{i-1}} & t_{i-1} \leqslant t \leqslant t_i \\ \dfrac{t_{i+1} - t}{t_{i+1} - t_i} & t_i \leqslant t \leqslant t_{i+1} \\ 0 & \text{otherwise} \end{cases}, \tag{2.9}$$

where the unknown coefficients γ_i, $i = 1 \ldots N$ are the new parameters that will be estimated to account for the control and N is the number of nodes along the time span analysed. The spread of the N nodes should be specified in the model. For simulations reflecting dynamics observed in the supine position we placed N with a frequency of 6–10 s, but during HUT, where dynamics change, significantly more points were added. It should be noted that the more points added to the time span, the longer the simulations will be.

2.2.4 *Nominal parameter values.* Literature values and subject-specific information were integrated to identify nominal values for all model parameters (resistances, capacitors, heart and HUT parameters) as well as to predict initial conditions for all state variables. Nominal parameter values were obtained by considering mean values for all pressures, flows and volumes in the system obtained while the subject was in the supine position (before HUT). The mean pressure in the upper arteries, $\bar{p}_{au}$, was estimated from data as the average pressure over the 'steady' portion of the pressure-time series (in the supine position). The resistance between any large arteries in the body is small (in the supine position); thus the mean pressure in the lower arteries $\bar{p}_{al}$ was estimated as 98% of $\bar{p}_{au}$. The same applies to the resistance between upper and lower body veins. Consequently, we set the upper body venous pressure $\bar{p}_{vu} = 3.5$, while the mean pressure in the lower body veins $\bar{p}_{vl} = 3.75$. Values for the total blood volume within each compartment were obtained as fractions of the total blood volume, which for healthy subjects can be predicted from Shoemaker (1989)

$$V_{tot} = \begin{cases} (3.47 \cdot \text{BSA} - 1.954)1000 & \text{Female} \\ (3.29 \cdot \text{BSA} - 1.229)1000 & \text{Male} \end{cases}, \tag{2.10}$$

where $\text{BSA} = \sqrt{lw/3600}$ denotes the body surface area, l (cm) denotes the height and w (kg) the weight of the subject studied. For each compartment, we used the stressed and unstressed blood volume as proposed by Beneken and DeWitt (1967). Values of stressed the blood volume are given in Table 2.

Cardiac output was estimated from the assumption that the entire volume is circulated in the body within 1 min (Ellwein, 2008). Alternative estimates for cardiac output could be derived as discussed in recent studies by Sun *et al.* (2009). Average flows between the upper and lower body were estimated utilizing the assumption that, for a subject in the supine position, 90% of the blood flows between upper

TABLE 2 *For each compartment volume is estimated as fractions of the total volume* V_{tot}, *and the total compartment blood volume is separated between a stressed and an unstressed volume, i.e.* $V_{\text{tot},i} = V_{\text{str},i} + V_{\text{un},i}$

Volume	Position	Fraction of total volume	Fraction of stressed volume
V_{au}	Upper body arteries	0.11	0.19
V_{al}	Lower body arteries	0.66	0.05
V_{vu}	Upper body veins	0.02	0.16
V_{vl}	Lower body veins	0.06	0.05

This table lists stressed volumes calculated as a fraction of the total volume. Values are computed using ideas proposed by Beneken and DeWitt (1967). In this study the upper body compartments contain arteries and veins in the head, thorax and abdomen, whereas the lower body compartments contain arteries and veins in the legs.

body arteries and veins, whereas 10% of the blood flow supports the vasculature in the lower extremities (Beneken and DeWitt, 1967).

Utilizing estimates for blood flow, pressure and volumes, values for model resistors and capacitors (compliances) can be found by rewriting the pressure–volume (2.2) and pressure–flow (2.4) relations as

$$R = \frac{\bar{p}_{\text{in}} - \bar{p}_{\text{out}}}{\bar{q}},$$
$$C = \frac{\bar{V} - \bar{V}_{\text{un}}}{\bar{p}} = \frac{V_{\text{str}}}{\bar{p}},$$

where $\bar{p}, \bar{q}, \bar{V}$ denote mean values for the respective blood pressures, flow and volumes, respectively. Subscripts '*un*' and '*str*' denote unstressed and stressed volumes, respectively. The stressed volume fractions are given in Table 2.

For the heart model, parameters representing the minimum and maximum elastance as well as timing of the pump function must be estimated. The minimum left ventricular elastance can be obtained from the pressure–volume relation (2.2), noting that when the left ventricular volume equals the end-diastolic volume (V_{ED}), we have

$$\bar{p}_{\text{pv}} = E_{\min}(V_{\text{ED}} - V_{\text{lh,un}}),$$

where $\bar{p}_{\text{pv}}$ denotes the pulmonary venous pressure. This pressure does not appear elsewhere in the model. We assumed that the pulmonary venous pressure is slightly higher (4 mmHg) than its systemic counter part (Tortora & Anagnostakos, 1990; Guyton & Hall, 1996). Similarly, the maximum left ventricular elastance can be predicted by assessing the same relation at the end-systolic phase. For this case

$$p_{\text{lh,sys}} = E_{\max}(V_{\text{ES}} - V_{\text{lh,un}}),$$

where $p_{\text{lh,sys}}$ denotes the maximal systemic arterial pressure (obtained from the data) and V_{ES} denotes the end-systolic volume. For both parameters, we assumed that the unstressed value of the ventricular volume $V_{\text{lh,un}} = 10$ ml, which was used in previous studies (e.g. Ellwein, 2008).

The timing of the pump is achieved via parameters T_M, T_R and T. For this study, we estimated T_M from data (for each cardiac cycle, we let T_M be the time at which the pressure wave reached its

TABLE 3 *Model parameters: the nominal parameter values and equations used for predicting them*

Name	Definition	Equation	Value	Units
V_{tot}	Total blood volume	Equation (2.10)	5377 ± 549	ml
l	Height		183 ± 8	cm
w	Weight		80 ± 10	kg
CO	Cardiac output	$V_{\text{tot}}/60$	90 ± 9	ml/s
$\bar{p}_{\text{au}}$	Upper body mean arterial bp	$\frac{1}{N}\sum_{i=1}^{N} p_{\text{au}}(i)$	68 ± 11	mmHg
$\bar{p}_{\text{al}}$	Lower body mean arterial bp	$0.98\,\bar{p}_{\text{au}}$	67 ± 11	mmHg
$\bar{p}_{\text{vu}}$	Upper body mean venous bp		3.5	mmHg
$\bar{p}_{\text{vl}}$	Lower body mean venous bp		3.75	mmHg
$\bar{q}_{\text{up}}$	Upper body flow	0.9 CO	81 ± 8	ml/s
$\bar{q}_{\text{low}}$	Lower body flow	0.1 CO	9.0 ± 0.9	ml/s
$R_{i,\text{op}}$	Small resistance, open valve		0.001	mmHg s/ml
$R_{i,\text{cl}}$	Large resistance, closed valve		20	mmHg s/ml
R_{aup}	Upper body peripheral resistance	$(\bar{p}_{\text{au}} - \bar{p}_{\text{vu}})/\bar{q}_{\text{up}}$	0.81 ± 0.19	mmHg s/ml
R_{alp}	Lower body peripheral resistance	$(\bar{p}_{\text{al}} - \bar{p}_{\text{vl}})/\bar{q}_{\text{low}}$	7.1 ± 1.6	mmHg s/ml
R_{al}	Upper body arterial resistance	$(\bar{p}_{\text{au}} - \bar{p}_{\text{al}})/\bar{q}_{\text{low}}$	0.15 ± 0.03	mmHg s/ml
R_{vl}	Lower body venous resistance	$(\bar{p}_{\text{vl}} - \bar{p}_{\text{vu}})/\bar{q}_{\text{low}}$	0.028 ± 0.003	mmHg s/ml
C_{au}	Upper body arterial compliance	$0.19\,\bar{V}_{\text{au}}/\bar{p}_{\text{au}}$	1.7 ± 0.4	ml/mmHg
C_{al}	Lower body arterial compliance	$0.05\,\bar{V}_{\text{al}}/\bar{p}_{\text{al}}$	0.26 ± 0.06	ml/mmHg
C_{vu}	Upper body venous compliance	$0.05\,\bar{V}_{\text{vu}}/\bar{p}_{\text{vu}}$	51 ± 5	ml/mmHg
C_{vl}	Lower body venous compliance	$0.16\,\bar{V}_{\text{vl}}/\bar{p}_{\text{vl}}$	4.3 ± 0.4	ml/mmHg
$\bar{p}_{\text{pv}}$	Mean pulmonary venous bp		4	mmHg
$\bar{p}_{\text{lh,sys}}$	Mean max systemic arterial bp	$\frac{1}{M}\sum_{i=1}^{M} p_{\text{au,sys}}(i)$	102 ± 13	mmHg
V_{ED}	End-diastolic volume		125	ml
V_{ES}	End-systolic volume		70	ml
$V_{\text{lh,un}}$	Unstressed ventricular volume		10	ml
E_{min}	Min elastance	$\bar{p}_{\text{pv}}/(V_{\text{ED}} - V_{\text{lh,un}})$	0.03	mmHg/ml
E_{max}	Max elastance	$\bar{p}_{\text{lh,sys}}/(V_{\text{ES}} - V_{\text{lh,un}})$	1.7 ± 0.2	mmHg/ml
T_R	Max elastance to relaxation	0.18/T	0.20 ± 0.01	N.D.
T_M	Time of max elastance	Data	0.11 ± 0.01	N.D.
T	Length of i'th cardiac cycle	Data	0.90 ± 0.07	s

$\bar{p}_{\text{au}}$ includes data from the supine portion of the blood pressure (bp) time-series ($t < 180$ s), and N denotes the number of points within this period. $\bar{p}_{\text{au,sys}}$ includes the systolic blood pressure values for the M periods found for $t < 180$. Values for venous blood pressure are from Goers *et al.* (2008).

maximum, whereas T_R was defined relative to the length of the cardiac cycle as $T_R = 0.19/T$ (Ottesen & Danielsen, 2003; Ellwein, 2008). Table 3 specifies parameter values for all model parameters.

Initial values for all differential equations, i.e. for all arterial and venous pressures, as well as the left ventricular volume were set as average values predicted as described above. These values can be found in Table 3 along with values for all nominal parameters.

2.3 *Model analysis*

The objective of this study is to use heart rate as an input and estimate model parameters allowing the model to fit arterial blood pressure data recorded at the level of the carotid sinus. The model will be applied to data obtained from five healthy young subjects in the supine position and during HUT. To do so, we first analysed the model dynamics, while the subjects were in the supine position, followed by the analysis of HUT. For the steady-state analysis, we first investigated the sensitivity of the carotid blood pressure to the model parameters, then we determined a set of identifiable parameters, and finally we used non-linear optimization to estimate the parameters. After obtaining base parameters representing steady-state dynamics, parameters being regulated by baroreflex regulation were estimated during HUT. Data analysed for this study include continuous heart rate and blood pressure measurements, as well as gender, age, height, and weight of the subjects. Previous studies by Ellwein (2008), Pope *et al.* (2009) have shown that parameter estimates obtained by minimizing the least squares error between computed and measured values of arterial pressure gave rise to models that underestimated cardiac output and total blood volume. These quantities are typically not measured. Consequently, to obtain a set of parameters providing realistic model estimates of cardiac output and blood volume, we used approximate values obtained using allometric scaling laws estimating blood volume as a function of height, weight, age and gender. The total blood volume was scaled by 85% to get the volume of the systemic circulation, and as discussed in (2.10) cardiac output was estimated by assuming that the total blood volume is circulated in 1 min.

The model developed in this study estimates blood pressure and flow as pulsatile quantities, but since the model is analogous to an RC-circuit, it does not allow for prediction of wave propagation; consequently direct comparison of computed and measured values of blood pressure is erroneous. To obtain adequate pulsatility, we identify model parameters that allow prediction of systolic and diastolic values of blood pressure. These values can be obtained from computing the maximum and minimum pressure within each cardiac cycle. However, the maximum and minimum functions are not smooth; consequently, we applied the smoothing function (Chen *et al.*, 2004)

$$\min_{\epsilon}(x) = -\epsilon \ln\left(\sum_i \exp(-x_i/\epsilon)\right)$$

for which $\epsilon > 0$ represents the degree of smoothness (large values of ϵ give rise to more smoothing) and x represents the vector (indexed by i) to be minimized (or maximized).

The allometric data estimating cardiac output and blood volume will be included in the model output while the subject is in the supine position, where these quantities are assumed approximately constant. During HUT and subsequent control these quantities vary and thus model output will only include systolic and diastolic arterial blood pressure. Consequently, the model output vector is given by

$$y_{\text{sup}} = [p_{\text{au,sys},1}, \ldots, p_{\text{au,sys},M}, p_{\text{au,dia},1}, \ldots, p_{\text{au,dia},M}, V_{\text{st},1}, \ldots, V_{\text{st},M}, \text{CO}_1, \ldots, \text{CO}_M]^{\text{T}}, \tag{2.11}$$

$$y_{\text{tilt}} = [p_{\text{au,sys},1}, \ldots, p_{\text{au,sys},M}, p_{\text{au,dia},1}, \ldots, p_{\text{au,dia},M}]^{\text{T}}, \tag{2.12}$$

where M is the number of cardiac cycles analysed and subscripts *sup* and *tilt* refer to supine and HUT simulations, respectively. Note, that quantities in y do not depend continuously on time, but represent one value for each cardiac cycle. Using y, we defined the residual vector R between computed (y^c) and

measured (y^d) quantities as

$$R = \frac{1}{\sqrt{K}} \left[\frac{y_1^c - y_1^d}{y_1^d}, \frac{y_2^c - y_2^d}{y_2^d}, \ldots, \frac{y_K^c - y_K^d}{y_K^d} \right]^{\mathrm{T}}, \tag{2.13}$$

where K is the length of the model output vector. For simulations representing supine dynamics $K = 4M$, the model residual (2.11) has four entries of length M, while for simulations during HUT $K = 2M$, the model residual (2.12) has two entries of length M. Since pressure, volume and cardiac output have different units, and since the data segments analysed may vary in length, we scaled the residual by the value of the measurements and by the square root of the number of samples K.

2.3.1 *Sensitivity analysis.* The first step in identifying a subset of parameters to be estimated, given available data, was to conduct sensitivity analysis and rank parameters from the most to the least sensitive. The base model contains $n = 12$ parameters as follows:

$$\theta = \{R_{\mathrm{aup}}, R_{\mathrm{al}}, R_{\mathrm{vl}}, R_{\mathrm{alp}}, C_{\mathrm{au}}, C_{\mathrm{al}}, C_{\mathrm{vl}}, C_{\mathrm{vu}}, T_R, E_{\min}, E_{\max}, V_{\mathrm{un,lh}}\}.$$

The sensitivity matrix is defined as

$$S = \frac{\partial R}{\partial \tilde{\boldsymbol{\theta}}}, \tag{2.14}$$

where $\tilde{\theta}$ denotes the log-scaled parameters and R denotes the residual vectors given in (2.11) and (2.12). Sensitivities were computed using the forward difference approximation

$$\frac{\partial y_k}{\partial \tilde{\theta}_i} = \frac{y_k(t, \tilde{\theta} + he_i) - y_k(t, \tilde{\theta})}{\delta}, \quad \text{where } e_i = \left[0 \ \ldots \ 0 \overset{i}{\hat{1}} 0 \ \ldots \right]^{\mathrm{T}}$$

is the unit vector in the ith component direction and $\delta = \sqrt{\chi}$ is the step size; $\chi = 10^{-8}$ is the integration tolerance used for solution of the dynamical system. We used a scaled two-norm to get the total sensitivity S_i to the ith parameter

$$S_i = \left(\frac{1}{K} \sum_{j=1}^{K} S_{i,j}^2 \right)^{1/2}. \tag{2.15}$$

Sensitivities are shown in Fig. 5.

2.3.2 *Subset selection.* As suggested in Olufsen & Ottesen (2012), we combined two approaches for estimating a subset of uncorrelated parameters. First, we note that the model contains two parallel circuits predicting flow in the upper and lower body. For the supine dynamics, the model could be reformulated as an equivalent circuit with one branch. Thus, parameters in one of the two branches will not be identifiable. We chose to analyse parameters representing compartments in the upper body, while we kept parameters in the lower body compartments (containing less blood volume) constant. The reduced parameter set includes parameters $\theta = \{R_{\mathrm{aup}}, C_{\mathrm{au}}, C_{\mathrm{vu}}, T_R, E_{\min}, E_{\max}, V_{\mathrm{lh,un}}\}$. Next, we used singular value decomposition and QR factorization to identify parameters. The sensitivity matrix defined in (2.14) was decomposed as $R'(\tilde{\theta}) = U \Sigma V^{\mathrm{T}}$, where $\tilde{\theta}$ are the log-scaled parameters, Σ is a diagonal

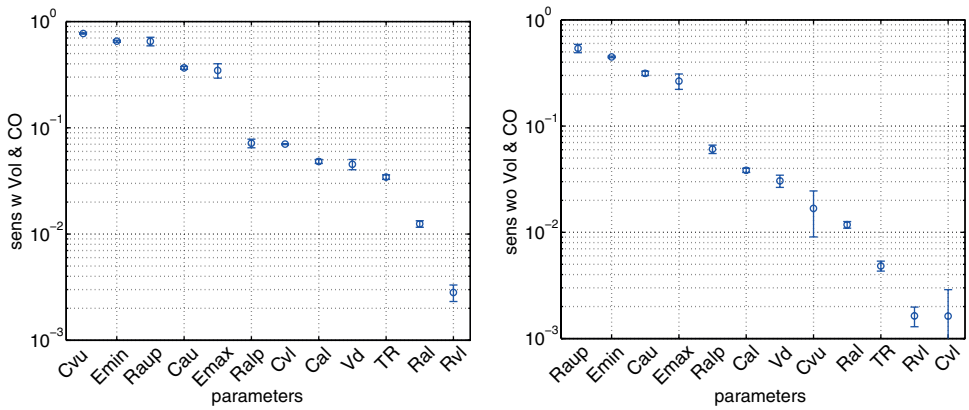

FIG. 5. Ranked sensitivities $\|\partial R/\partial\tilde{\theta}\|_2$ plotted on a log scale. Values are displayed from the most to the least sensitive parameter. Left panel shows sensitivities estimated using (2.11) and right panel shows those estimated using (2.12).

matrix containing the singular values σ_i of R' and V is the associated right eigenvector. The number of identifiable parameter values can be found by predicting the numerical rank ρ of R'. Given a tolerance ϵ, the numerical rank of the matrix is the largest k such that the singular values $\sigma_{n-k+1} > \epsilon\sigma_n$. For our study $\epsilon = \sqrt{\chi}$, the square root of the integration tolerance χ. Using ρ, the matrix of eigenvectors V can be written as $[V_\rho \; V_{n-\rho}]$. The parameters associated with the ρ highest eigenvectors are then found using QR decomposition with column pivoting. It should be noted that the QR decomposition is not unique, but differs with the concrete implementation of the algorithm. However, for a given ρ the algorithm will return a set of ρ identifiable parameters. Independent of the exact algorithm, the subset is found by ${V_\rho}^{\mathrm{T}}P = QR$, where Q is an orthogonal matrix, and the first ρ elements of R form an upper triangular matrix with diagonal elements in decreasing order. The permutation matrix P can be used to reorder the parameter vector $\hat{\theta} = P^{\mathrm{T}}\theta$. Finally, the partition $\hat{\theta} = \{\hat{\theta}_\rho, \hat{\theta}_{n-\rho}\}$, where $\hat{\theta}_\rho$ contains the first ρ sensitive elements, while the vector $\hat{\theta}_{n-\rho}$ contains parameters that cannot be identified. In this study, these were kept at their nominal parameter values. The latter does introduce bias in the computations, but reduces the variance. At the same time estimation of only sensitive parameters makes the estimation algorithm more robust (Dochain & Vanrolleghem, 2001; Ipsen *et al.*, 2011). For this study, we performed subset selection for the reduced parameter set noted above by analysing the sensitivity matrix over the entire 180 s interval. This analysis was repeated for all five datasets for each of the two residuals. For the residual in (2.11), results show that independent of the dataset studied four parameters could be estimated including $\hat{\theta}_\rho = \{R_{\mathrm{aup}}, C_{\mathrm{au}}, C_{\mathrm{vu}}, E_{\mathrm{min}}\}$, while for the residual in (2.12) only two parameters can be estimated $\hat{\theta}_\rho = \{R_{\mathrm{aup}}, E_{\mathrm{min}}\}$.

This parameter set was tested further, by computing pair-wise correlations. To do so we use the model Hessian defined by $\mathcal{H} = S^{\mathrm{T}}S$, where S is the sensitivity matrix defined in (2.13). Using $\mathcal{H}$, the correlation matrix c can be computed as

$$c_{i,j} = \frac{C_{i,j}}{\sqrt{C_{i,i}C_{j,j}}}, \quad C = \mathcal{H}^{-1}.$$

The correlation matrix c is symmetric with 1's in the diagonal. All off-diagonal elements have values between $-1 \leqslant c_{i,j} \leqslant 1$; absolute values close to 1 indicate that parameters are correlated

(Olufsen & Ottesen, 2012). Moreover, it should be noted that c cannot be computed if $\mathcal{H}$ is singular. The aim here was to investigate correlations among parameters chosen by subset selection. For this subset, $\mathcal{H}$ is not singular, and thus c can easily be computed. For either parameters, the entries $c_{i,j}$ are close to 1, indicating that all parameters in the subsets are identifiable. It should be noted that all analysis methods presented here are local and only valid in a region close to the parameter values investigated, i.e. results may change as the parameters change. To ensure that optimized parameters were not correlated, this analysis should be repeated for the optimized parameter values.

2.3.3 *Parameter estimation.* Non-linear optimization was employed to estimate a set of model parameters that minimize the least squares error between the measured data and the model. This formulation relies on the assumption that the measurements can be described fully by the underlying model plus an error term representing the measurement noise, i.e. we assume that

$$y_{d,i} = y_m(t_i; \theta_\rho, \theta_{n-\rho}) + \epsilon_i, \quad i = 1, 2, \ldots, K,$$

where K denotes the number of elements in the output vector. For formulation of the statistical model, we assume that the errors ϵ_i are independent identically distributed (i.i.d.) random variables with mean $E[\epsilon_i] = 0$, covariance $\text{cov}(\epsilon_i, \epsilon_j) = 0$ and constant variance $\text{var}[\epsilon_i] = \mu^2$. Given this form of the statistical model, the objective function can be defined using the sum of least squares errors

$$\theta_{\text{opt},\rho} = \arg\min_{\theta_\rho} J(\theta), \quad J(\theta) = R^{\mathrm{T}}R = \frac{1}{K}\sum_{i=1}^{K}\left|\frac{y(t_i; \theta_\rho, \theta_{n-\rho}) - y_i}{y_i}\right|. \tag{2.16}$$

The scaling with y_i is included to ensure that all quantities in the output vector can be compared. Note that only parameters in the subset θ_ρ will be estimated, while parameters that are not identifiable $\theta_{n-\rho}$ remain constant at the nominal parameter values. The identifiable parameters θ_ρ were estimated using the Levenberg–Marquadt optimization algorithm (Kelley, 1999). Upper and lower bounds were set for all model parameters. For simulations presented here, we allowed parameters to increase or decrease by a factor of 4 from nominal parameter values.

As outlined below, model parameters were estimated first in the supine position, and then during HUT.

(1) First, we estimated one value for each of the identifiable parameters during the supine position for $t = 0$–180 s. For this simulation, we solved the minimization problem in (2.16) using the residual defined in (2.11) providing optimal values $\hat{\theta}_\rho = \{\hat{R}_{\text{au}}, \hat{C}_{\text{au}}, \hat{C}_{\text{vu}}, \hat{E}_{\text{min}}\}$.

(2) Second, over the same interval we estimated time-varying parameters as described in (2.9). As in step 1, we solved (2.16) using the residual defined in (2.11) providing optimal values $\hat{\theta}_\rho = \{\hat{\gamma}_{R_{\text{au}},i}, \hat{\gamma}_{C_{\text{au}},i}, \hat{\gamma}_{C_{\text{vu}},i}, \hat{\gamma}_{E_{\text{min}},i}\}$. To understand the impact of varying parameters in time, we repeated this simulation three times, including one value for each parameter for each 6, 8 and 10 s of data, i.e. we estimated $4 \times \eta$ parameters for $\eta = (18, 23, 30)$.

(3) Then we simulated the gravitational pooling of blood in the legs occurring as a response to HUT. Initial values for this simulation were assigned to the optimal values predicted in step 1. HUT simulations were compared against 180 s of data for $t = 110$–290 s. Note that this interval overlaps with the interval used for predicting supine dynamics.

TABLE 4 *Optimized parameter values found in the supine position*

Parm	Init 1 sub	Opt 1 sub	Opt (time-var)	Init 5 sub	Opt 5 sub	Unit
R_{aup}	0.81	0.86	0.89 ± 0.18	0.82 ± 0.19	0.89 ± 0.18	mmHg s/ml
C_{au}	1.64	2.3	1.4 ± 0.5	1.8 ± 0.4	1.4 ± 0.5	ml/mmHg
C_{vu}	53	67	69 ± 7	54 ± 9	69 ± 7	ml/mmHg
E_{min}	0.03	0.014	0.015 ± 0.002	0.027 ± 0.007	0.015 ± 0.002	mmHg/ml

The first three columns give results for one representative subject, while columns 4–5 give results averaged over all five subjects.

(4) Finally, we modelled blood pressure regulation by varying parameters representing vascular resistance and cardiac contractility in time as discussed above and in step 2. For this optimization problem, we used (2.9) to make parameters time-varying and solved (2.16) using the residual defined in (2.12). This optimization determined optimal values $\hat{\theta}_\rho = \{\hat{\gamma}_{R_{au},i}, \hat{\gamma}_{E_{min},i}\}$.

3. Results

Following the steps outlined above, we first show results obtained for a subject in the supine position followed by results obtained when the same subject was exposed to a HUT test.

3.1 *Optimization during the supine position*

For simulations estimating the supine dynamics, we used heart rate and blood pressure data from the first 180 s of the time series (see Fig. 1e). The estimates of patient-specific parameters were obtained using two approaches; first, we estimated one set of parameters over the entire 180 s of data; second, we allowed model parameters to vary slowly in time. The latter was done using the approach outlined in Section 2.2.3. Moreover, to ensure that results were similar for measured and calculated carotid artery data, simulations were repeated (with one parameter per 8 s) for both datasets. Finally, Table 4 gives a comparison of mean values obtained over all five datasets. Results comparing simulations with the measured carotid data are shown in Fig. 6. Results with calculated carotid data were not significantly different and are thus not shown. Generally, we found that better results are obtained when parameters were allowed to vary slowly in time; cf. Fig. 6a and e. Both simulations gave the same mean value predictions for p_{au}, though with time-varying parameters the model was able to capture fast and slow (likely due to respiration) oscillations. Figure 6a shows results obtained while estimating one set of parameters of the entire 180 s of data, and Fig. 6e shows results when parameters vary slowly in time. For each of the two simulations, the second column of Fig. 6 shows a 5-s segment from $t = 82-89$ s. The third and fourth columns of Fig. 6 show data versus computed values of diastolic and systolic pressures, respectively. It should be noted that time-varying parameters are needed to accurately predict systolic and diastolic pressures, for these simulations $R^2 = 0.65$ and $R^2 = 0.77$.

One limitation of the results reported here is that estimated compliance values reflect that the pulse wave is measured in a peripheral vessel, rather than in the carotid artery. Consequently, compliance values may be too small compared with expected values in the central vessels. However, all other quantities (pressures, volumes and flows) estimated by the model were physiologically reasonable.

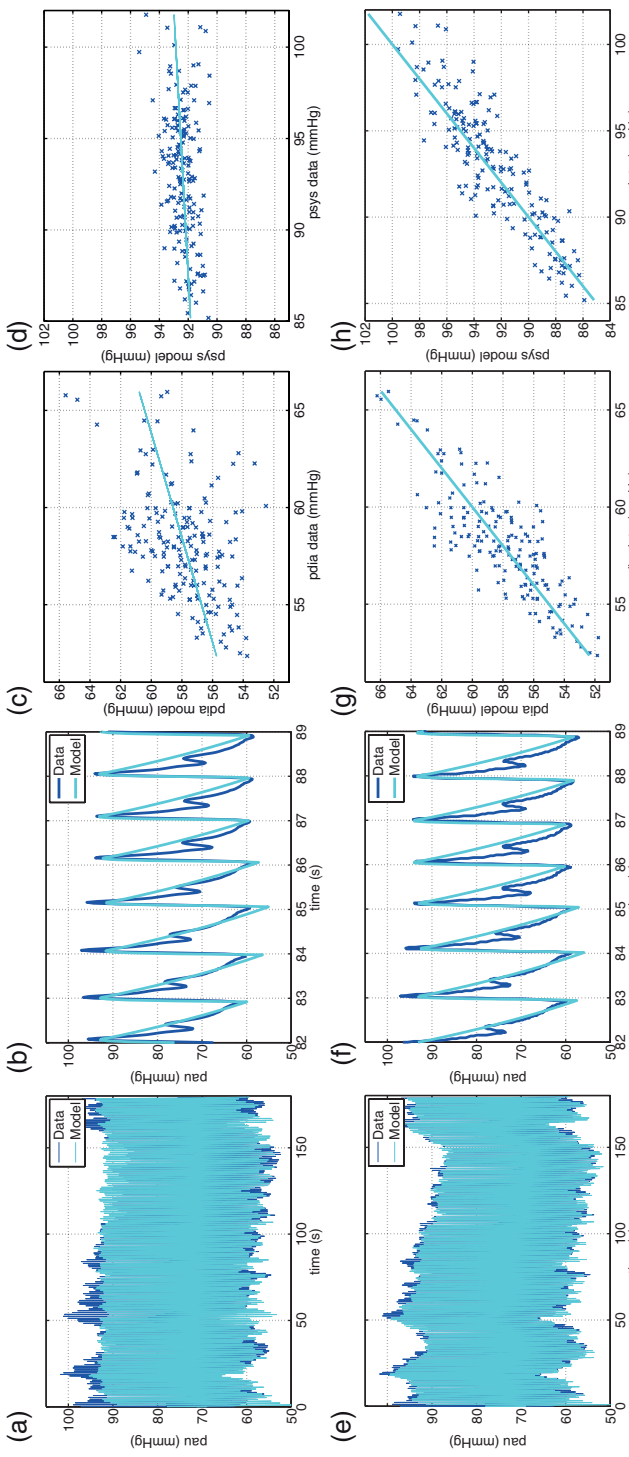

FIG. 6. (a) The measured upper body arterial blood pressure (dark line) and the optimized model output (light line) in the supine position (over a 180 s time span); (b) a zoomed portion of (a) for $t = 82$–89 s. (c) and (d) Model versus computed values for diastolic and systolic pressures, respectively, where the light line shows the best one-to-one fit between the computed and measured values. Ideally, the dots should lie on a straight line with slope 1. (e–h) The same as (a–d), respectively, but obtained by estimating time-varying parameters. With time-varying parameters (g–h) $R^2 = 0.65$ (diastolic) and $R^2 = 0.77$ (systolic), compare diastolic and systolic computed outcomes to their respective expected outcomes.

3.2 *HUT optimization*

Figure 8a shows the measured and calculated blood pressure and the corresponding model output for a representative subject tilted to 60°. This result represents dynamics without blood pressure regulation, i.e. it was obtained by keeping all parameters constant at optimized values obtained in the supine position. Results were obtained by accounting for hydrostatic pooling of blood in the legs as described in (2.8). The arterial blood pressure drops during HUT and remains low for the duration of the simulation. Figure 8b and c shows that when parameters R_{aup} and $E_{\min}$ (shown in Fig. 8e and h) were controlled, the model was able to fit the observed pressure. The result in Fig. 8b was obtained by estimating the time-varying model parameters $\theta_{\text{ctr}} = \{\gamma_{R_{\text{aup}},i}, \gamma_{E_{\min},i}\}$, minimizing the least squares error between measured and modelled carotid blood pressure, while the result in Fig. 8c reflects comparison with the calculated carotid data as given in (2.1). Results in Fig. 8f and i show diastolic and systolic model predictions plotted against data. The cyan line with slope 1 indicates the unity between the model and data. The top row in Fig. 9 shows results obtained for all five subjects comparing model results against measured carotid data. The bottom two rows (cyan line) of Fig. 9 show piecewise linear predictions of peripheral resistance R_{aup} and minimum elastance $E_{\min}$, whereas Fig. 10 shows pooled predictions of R_{aup} and $E_{\min}$ for all five datasets. On the basis of these fits, we propose to model the change in these quantities using combinations of Hill and polynomial functions given by

$$X(t) = \begin{cases} X_{\min,ss} & t \leqslant t_{\text{tilt}} \\ X_{\min,ss} - (X_{\min,ss} - X_{\min,m}) \dfrac{(t - t_{\text{tilt}})^n}{X_{\min,h}^n + (t - t_{\text{tilt}})^n} & t > t_{\text{tilt}} \end{cases}$$

$$Y(t) = A(t - t_1)^{k_1}(t_2 - t)^{k_2}, \quad A = \frac{-B}{(t_2 - t_1)/2)^{(k_1+k_2)}},$$

where $X_{\min,i}, t_{\text{tilt}}, n, B, k_1, k_2, t_1, t_2$ are model parameters. The minimum elastance $E_{\min}$ is predicted using $X(t)$ and the peripheral resistance by combining the expressions for X and Y. Predictions of arterial pressure at the level of the carotid using these functions are shown in the second row of Fig. 9. Note that the functions predict the steady level and transition during tilt fairly well, but neglect the faster variation within these periods. Hence, these functions capture the overall trend in the dynamical responses but ignore the faster variations captured by the piecewise linear functions.

The significance of the model was corroborated further by examining dynamics of quantities for which data are not available. Starting at the heart, the volume and cardiac output for a representative subject are depicted in Fig. 11. The ventricular volume (Fig. 11a and b) is within normal physiological bounds for a healthy person (Møgelvang *et al.*, 1986). Moreover, consistent with observations in the literature (Melbin *et al.*, 1982; Ottesen & Danielsen, 2003; Feher, 2012), the CO is decreased slightly when the blood pressure regulation is inhibited as depicted in Fig. 11c. However, when the blood pressure regulation is engaged, CO is increased after the onset of HUT and then returns to the values before HUT as seen in Fig. 11d.

Figure 12 shows the lower body arterial p_{al} and venous p_{vl} pressure, the upper body venous pressure p_{vu}, as well as the flow between the upper and lower body on the arterial q_{al} and venous q_{vl} side for a representative subject. We also show the dynamics of resistance between the upper and lower body on the venous side R_{vl}. These figures represent dynamics observed during HUT, i.e. model parameters are time-varying. Immediately upon HUT flow from the lower to upper body veins stops, as the venous valve closes, preventing return flow in the leg veins. As a result flow to the lower body is reduced.

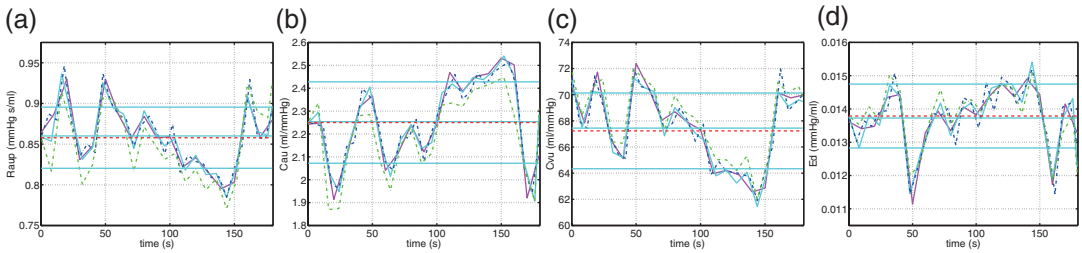

FIG. 7. The graphs show the four parameters in the subset that were estimated as time-varying parameters in the supine position including (a) upper body peripheral resistance R_{aup}, (b) upper body arterial compliance C_{au}, (c) upper body venous compliance C_{vu} and (d) minimum ventricular elastance E_{min}. The 'zig–zag' lines show the results obtained with 6-s (blue dashed), 8-s (cyan solid) and 10-s (magenta solid) intervals, respectively, against the measured carotid data, whereas the dashed green line shows results obtained with the calculated carotid data. Note, colours can only be seen online. The solid horizontal lines show mean values and standard deviations for the estimation of the time-varying parameters, and the dashed horizontal red line shows the results obtained when estimating one value over the entire period.

These observations agree with those found in the literature (Enishi *et al.*, 2004). Similar observations were made for all five datasets.

Simulations shown above were obtained by regulating two quantities R_{aup}, and E_{min}, while $R_{alp} = kR_{aup}$. Results show that similar dynamics were obtained for all five datasets. Moreover, it should be noted (cf. Figs 7 and 10) that the parameters estimated during HUT (Fig. 10) vary by orders of magnitude, while in the supine position (Fig. 7) they only varied slightly. Finally, it should be noted that, during HUT, none of the compliance parameters was included in the parameter estimation; these are only identifiable when cardiac output and blood volume are included in the least squares cost (2.16). During supine position we used the residual in (2.11), but during HUT, the blood volume and cardiac output are expected to vary; thus we cannot include our pseudo data estimating overall values for the subject in question. Thus, during HUT identifiability was done using the residual in (2.12) giving rise to a subset without compliance parameters.

4. Discussion and conclusion

Our study has provided an approach to examine cardiovascular regulation during HUT. This was done by developing a five-compartment model that uses heart rate as an input to estimate pulsatile values of blood flow, pressure and volume. HUT was imposed by including gravitational pooling of blood in the legs, and the autonomic response to HUT was included via time-varying parameters estimating vascular resistance and cardiac contractility. Non-linear optimization minimizing the least squares error between measured and computed values of systolic and diastolic blood pressure was used to estimate the time-varying model parameters. The model was compared with measured and calculated values for cardiac blood pressure for five healthy young adults.

Results showed (see Figs 6–9) that the model was able to fit measured and calculated carotid blood pressures in the supine position and during HUT. We noted, as expected that parameter variation during HUT is significantly larger than in the supine position (cf. Figs 7 and 10). On the basis of these observations, we hypothesize that the large changes observed in Fig. 10 are due to cardiovascular regulation of these targets, while comparatively small variations observed in Fig. 7 (summarized in Table 4) is a result of variation due to respiration (Triedman & Saul, 1994). During inspiration the lungs are filled with air, causing the diaphragm to lower; as a result the transmural pressure in the upper-body arteries

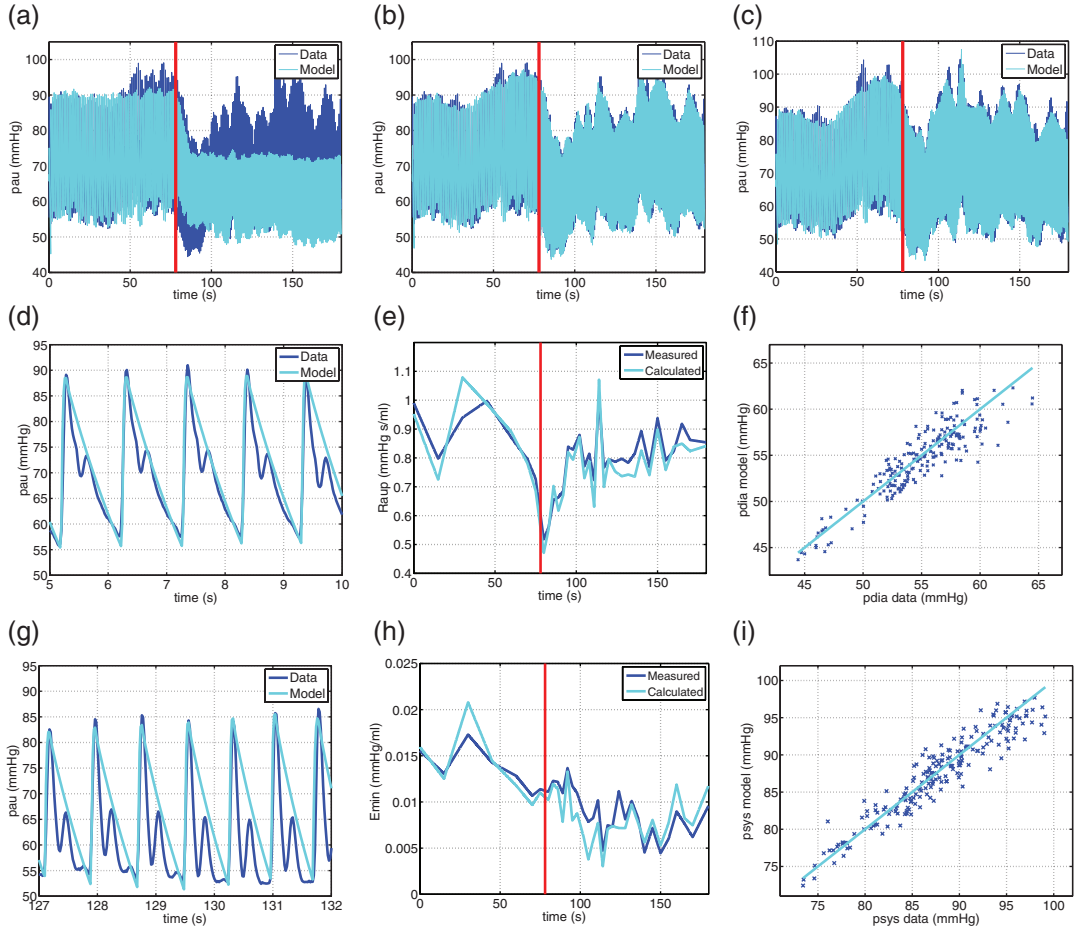

FIG. 8. (a) The measured upper body arterial blood pressure and the model output for a subject tilted over a 180 s time span, without parameters impacted by cardiovascular regulation; (b) the same quantities as (a) where parameters impacted by cardiovascular regulation are estimated as described in (2.9); (c) the same as (b) using the calculated carotid pressure (2.1). (d) and (g) zoomed portions of (b) for $t = 0$–5 s and $t = 127$–132 s, respectively; (e) and (h) optimized values for R_{aup} and E_{min}. The dark blue line shows results obtained optimizing against measured carotid data (b) and the light cyan line against calculated carotid pressure (c). Finally, (f) and (g) predictions of diastolic ($R^2 = 0.83$) and systolic ($R^2 = 0.87$) pressure for (b). The vertical red line indicates the onset of HUT.

and veins decrease. This decrease in tissue pressure is likely to impact the compliance and resistance of the vessels. Similarly, it is likely that cardiac contractility is decreased during inspiration. However, assuming that no controls are operating while the subject is in the supine position is not realistic. The control system is continuously active (Robertson *et al.*, 2004). In addition, other quantities estimated by the model, including cardiac output, pressures in the other compartments and blood volumes, were all reasonable compared with values reported in the literature (Guyton & Hall, 1996; Goers *et al.*, 2008).

To model the regulation during HUT, we varied upper and lower body resistance (R_{aup} and $R_{\text{alp}} = kR_{\text{aup}}$) and minimum elastance of the left heart (E_{min}). These quantities were modelled as piecewise linear time-varying functions, represented by a set of nodes $\gamma = \{\gamma_{R_{\text{aup}},i}, \gamma_{E_{\text{min}},i}\}$ as described in (2.9).

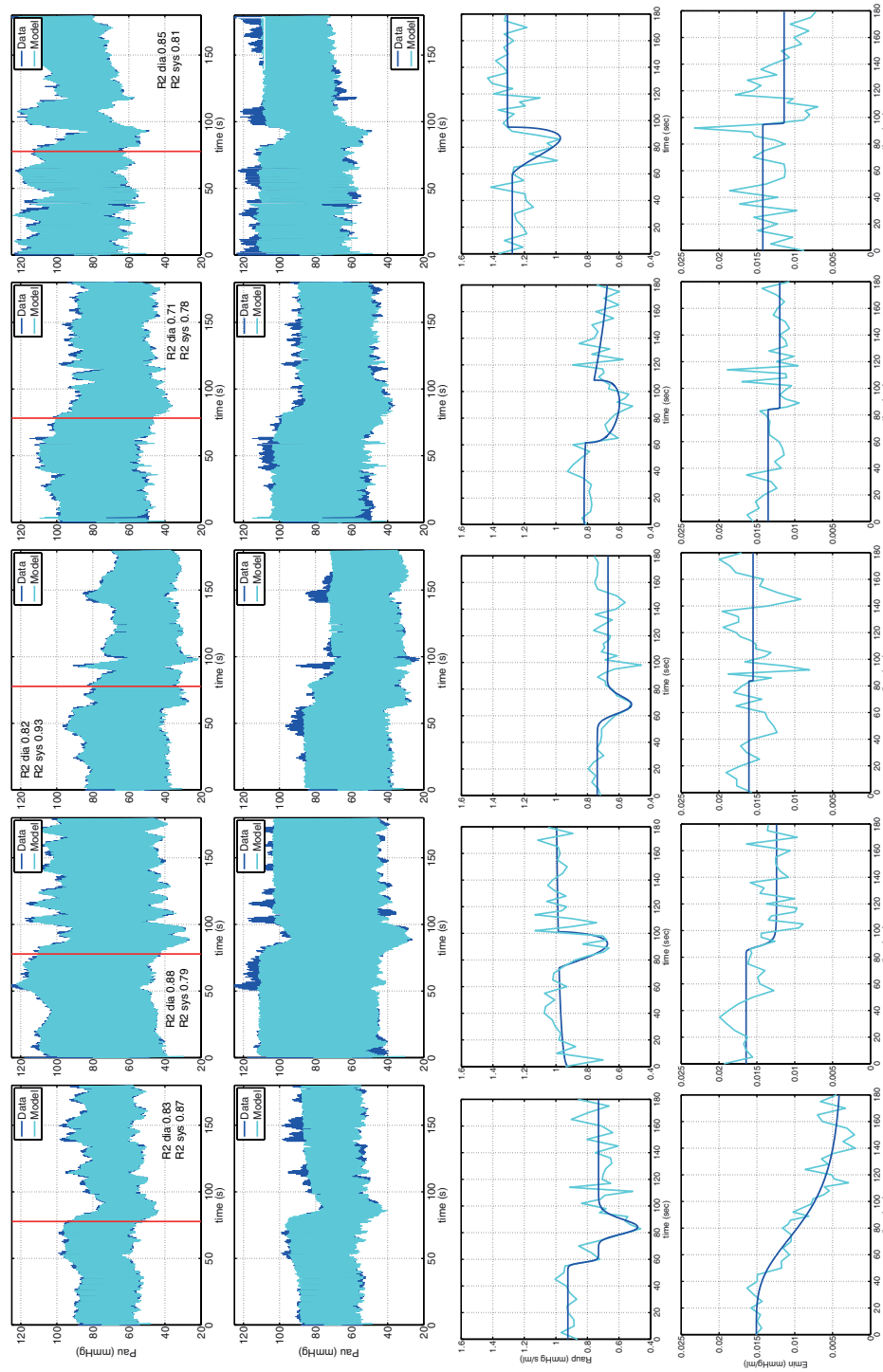

FIG. 9. Results showing computed and measured carotid blood pressure for five subjects included in the study. Top row shows results predicting time-varying parameters using piecewise linear functions, the second row shows results predicting arterial blood pressure using functional expressions for R_{aup} and E_{min}, the bottom two rows show predictions of R_{aup} and E_{min}. For each subject, R^2 values are marked on the graphs. The vertical red lines (top row) marks the onset of the tilt.

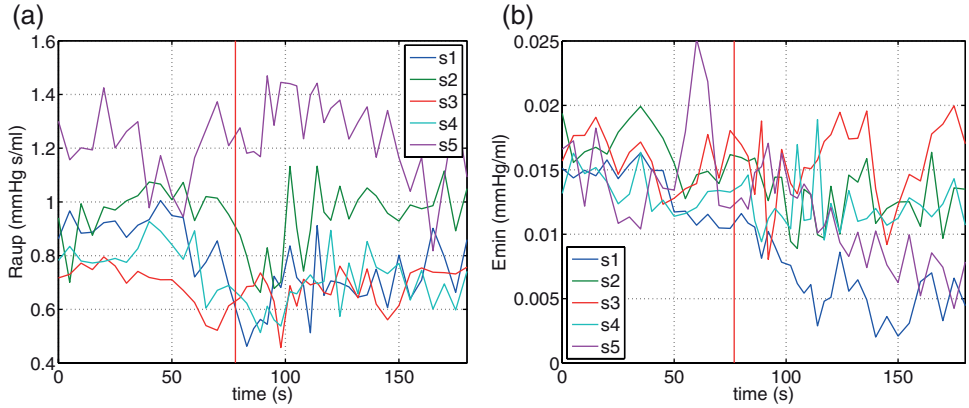

FIG. 10. Estimated values for upper body resistance R_{aup} and minimum contractility E_{min} for all five subjects.

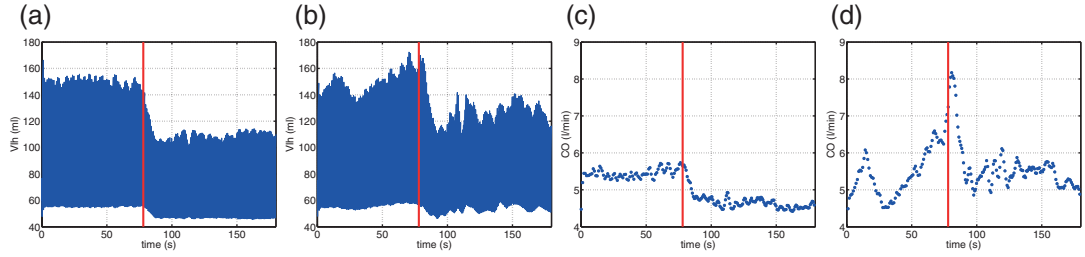

FIG. 11. First two graphs show ventricular volume during HUT without (a) and with (b) cardiovascular regulation. The associated cardiac output is shown in (c) and with (d). The vertical lines mark the onset of HUT.

Results showed that immediately upon HUT, peripheral resistance dropped. This drop could be related to the muscle action (Sprangers *et al.*, 1991; Wieling *et al.*, 1996) or be a consequence of changes in hydrostatic pressure in the compartment below the heart. The latter is more likely, since the HUT manoeuvre is executed in a relaxed fashion, and no massive muscle action is provoked. After the initial drop, arterial peripheral resistance increased due to contraction of smooth muscles in the muscular and the elastic arteries, respectively, secondary to increased nerve traffic in the sympathetic efferent nerves. Sympathetic nerve activation also has a positive inotropic effect on the heart, decreasing the left ventricular elastance and allowing the heart to pump more blood through the system.

Owing to changes in arterial resistance, blood volume is redistributed between the lower and upper body. Owing to the increased hydrostatic pressure in the dependent regions during HUT, blood volume increases more in the lower body than in the upper body, which results in ∼25% reduction of ventricular blood volume as described by Smith & Ebert (1990) and Matzen *et al.* (1991). The reduction in ventricular volume is paralleled by a significant drop in stroke volume as shown by Enishi *et al.* (2004) and van Lieshout *et al.* (2011). Similar results were also observed in previous modelling studies (Danielsen, 1998; Ottesen & Danielsen, 2003; Olufsen *et al.*, 2005; Ellwein, 2008).

It should be noted that we controlled R_{aup} and R_{alp}. The need to control the upper body resistance stems from the fact that vessels in the abdomen including the gut, liver and kidney were included in

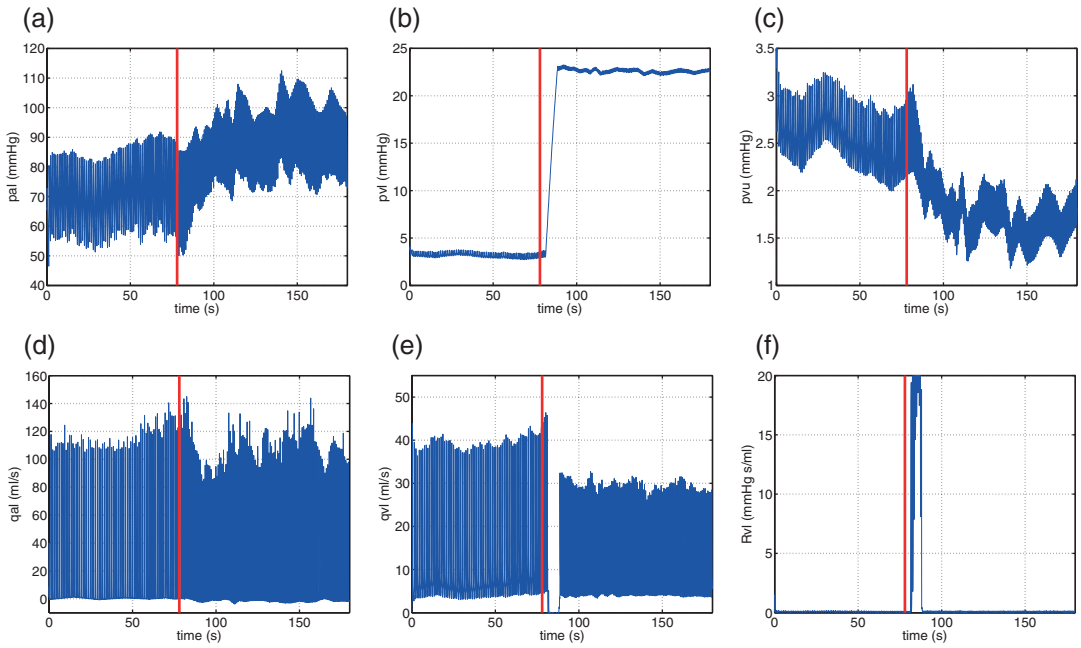

FIG. 12. (a) Pressure in the lower body arteries; (b) pressure in the lower body veins; (c) pressure in the upper body veins; (d) flow from upper to lower body arteries; (e) flow from lower to upper body veins; (f) resistance between lower and upper body veins. The vertical lines mark the onset of HUT.

the upper body. It is likely that if we had distinguished differently between the upper and lower body, by moving these vessels to the lower body it would be adequate to control R_{alp}, though the concept presented in this study would be directly transferable to a model with redistributed volumes.

As the model shows, through regulation of the selected quantities, blood pressure at the carotid bifurcation returns to homoeostatic levels after HUT, in line with the notion that the carotid baroreceptors dominate the blood pressure regulation in humans (Harms *et al.*, 2003; van Lieshout *et al.*, 2011). Another key observation is that with regulation of the model parameters, cardiac output increases after the onset of HUT and then returns to homoeostatic levels, which would also be expected as the metabolic demands in the passive upright position should be of the same magnitude as in the supine state. This agrees to some extent with results reported in the literature. Enishi *et al.* (2004) reported a slight decrease in cardiac output 1 min after HUT, whereas Harms *et al.* (2003) as well as van Lieshout *et al.* (2011) reported larger drops in cardiac output; their results though were reported for a subject being tilted for 10 and 20 min, respectively. Further proof of the significance of the model is given when examining other variables in the model where the left ventricular volume decreases when the tilt is performed in response to the decrease in filling pressure, which is also seen experimentally (Enishi *et al.*, 2004). The estimated venous pressure (p_{vl}) increases in the lower compartment as previously shown by others (Kegler *et al.*, 2001; Groothuis *et al.*, 2008), while the central venous pressure drops; again our results are similar to those reported in the literature (Harms *et al.*, 2003; van Lieshout *et al.*, 2011).

Moreover, we showed that, by prescribing E_{min} and R_{aup} by simple functions, it is possible to predict general trends in arterial blood pressure, while the minor oscillations could not be predicted, these may be a result of respiration, or represent the so-called Mayer-waves (Ottesen, 1997). It should be noted

that these secondary oscillations are more pronounced while the subject is tilted than in the supine position, which is in agreement with the observations reported and analysed by Ottesen (1997). The results confirm our observations that during tilt, peripheral resistance drops and then returns to the value before the tilt, or is slightly increased, while the minimum elastance is reduced slightly.

One limitation of our study is that heart rate was an input to the model, and thus, the model mainly predicts the impact of sympathetic regulation via estimation of cardiac contractility and vascular resistance. In future studies, one could consider including a model predicting heart rate e.g. as was done by Olufsen *et al.* (2008, 2006), Ottesen (1997), Olufsen & Ottesen (2012) and Bugenhagen *et al.* (2010). Moreover, if this approach is used for a larger population study, the validity of values used for parameters not estimated should be analysed further. In this study, we used 'text-book' values valid for the healthy young male; however, they would not be valid for all population groups. For example, values for venous pressure may be too low, and the assumption that the entire blood volume is circulated in a minute, used to obtain an estimate for cardiac output may not hold in general. One way to circumvent this last assumption is by including the measurement of cardiac output while the subject is in the supine position. Finally, it should be noted that the small secondary waves present in the blood pressure data cannot be reproduced by our model in its present state. These waves arise from the reflection of the pulse wave from the periphery, a phenomenon not included in our model. Such effects could be included in a number of ways, either by developing a lumped parameter wave propagation model from Womersley theory as suggested by Huberts *et al.* (2011), or by using empirically derived non-linear capacitors as suggested by Segers *et al.* (2001), though both of these ideas lead to a more complex model. While adding effects of wave propagation are important for many applications, e.g. for the study of wave propagation in normal and pathological arterial networks or for studies designed to analyse modulating the coronary perfusion pressure, the inclusion of wave reflections is most likely of little importance in the cardiovascular control system.

Funding

This work was supported in part by the NIH (NG/NIGMS P50-GM094503), National Science Foundation (DMS-0616597 and DMS-0636590), Carpenter Sophus Rasmussen Foundation and the Velux Foundation, Denmark. REU students were supported by the National Science Foundation (DMS-0636568, DMS-0552571 and DMS-1063010) and the National Security Agency (H9823-10-1-0252).

References

Abboud, F. M., Eckberg, D. L., Johannsen, U. J. & Mark, A. L. (1979) Carotid and cardiopulmonary baroreceptor control of splanchnic and forearm vascular resistance during venous pooling in man. *J. Physiol.*, **286**, 173–184.

Banks, H. T., Davidian, M., Samuels, J. R. & Sutton K. L. (2009) An inverse problem statistical methodology summary. *Mathematical and Statistical Estimation Approaches in Epidemiology* (G. Chowell, J. M. Hyman, L. M. A. Bettencourt & C. Castillo-Chavez eds). Dordrecht, The Netherlands: Springer.

Batzel, J. J., Goswami, N., Lackner, H. K., Roessler, A., Bachar, M., Kappel, F. & Hinghofer-Szalkay, H. (1999) Patterns of cardiovascular control during repeated tests of orthostatic loading. *Cardiovasc. Eng.*, **9**, 134–143.

Bauernschmitt, R., Schulz, S., Mehmanesh, H., Vahl, C. F. & Lange, R. (1999) Simulation of baroreflex control in a pulsatile mathematical model of the human arterial circulation. *Comp. Cardiol.*, **26**, 229–232.

Beneken, J. & DeWitt, B. (1967) A physical approach to hemodynamic aspects of the human cardiovascular system. In *Physiological Bases of Circulatory Transport: Regulation and Exchange* (B. Reeve and A. C. Guyton eds). Philadelphia: W.B Saunders Co, pp. 1–45.

Bugenhagen, S. M., Cowley, A. W. & Beard, D. A. (2010) Identifying physiological origins of baroreflex dysfunction in salt-sensitive hypertension in the Dahl SS rat. *Physiol. Genomics*, **42**, 23–41.

Chen, X., Qi, L. & Teo, K.-L. (2004) Smooth convex approximation to the maximum eigenvalue function. *J. Global. Opt.*, **30**, 253–270.

Chen, Z., Purdon, P. L., Brown, E. N. & Barbieri, R. (2010) A differential autoregressive modeling approach within a point process framework for non-stationary heartbeat intervals analysis. *Conf. Proc. IEEE Eng. Med. Biol. Soc.*, **2010**, 3567–3570.

Cintron-Arias, A., Banks, H. T., Capaldi, A. & Lloyd, A. L. (2009) A sensitivity matrix based methodology for inverse problem formulation. *J. Inv. Ill-Posed Problems*, **17**, 545–564.

Danielsen, M. (1998) Modeling of feedback mechanisms which control the heart function in a view to an implementation in cardovascular models. *Ph.D. Thesis*, Department of Mathematics, Roskilde University, Denmark.

Dochain, D. & Vanrolleghem, P. A. (2001) *Dynamical Modelling and Estimation in Wastewater Treatment Processes*. London, UK: IWA Publishing.

Eckberg, D. L. (2008) Arterial baroreflexes and cardiovascular modeling. *Cardiovasc. Eng.*, **8**, 5–13.

Ellwein, L. M. (2008) Cardiovascular and respiratory regulation, modeling and parameter estimation. *Ph.D. Thesis*, Department of Mathematics, North Carolina State University.

Enishi, K., Tajima, F., Akimoto, H. & Mita, R. (2004) Initial drop of blood pressure during head-up tilt in patients with cerebrovascular accidents. *Environ. Health. Prev. Med.*, **9**, 228–233.

Feher, J. (2012) *Quantitative Human Physiology: An Introduction*. Waltham, MA: Academic Press.

Fink, M., Batzel, J. J. & Kappel, F. (2004) An optimal control approach to modeling the cardiovascular-respiratory system: an application to orthostatic stress. *Cardiovasc. Eng.*, **4**, 27–38.

Fung, Y. C. (1996) *Biomechanics Circulation*. New York, NY: W.B. Springer.

Goers, T. A., Klingensmith, M. E., Chen, L. E. & Glasgow, S. C. (2008) *The Washington Manual of Surgery*. Philadelphia, PA: Wolters Kluwer Health/Lippencott Williams & Wilkins.

Groothuis, J. T., Poelkens, F., Wouters, C. W., Kooijman, M. & Hopman, M. T. E. (2008) Leg intravenous pressure during head-up tilt. *J. Appl. Physiol.*, **105**, 811–815.

Guyton, A. C., Coleman, T. G. & Granger, H. A. Overall regulation. *Ann. Rev. Physiol.*, **34**, 13–44.

Guyton, A. C. & Hall, J. E. (1996) *Textbook of Medical Physiology*. Philadelphia, PA: W.B. Saunders.

Harms, M. P. M., van Lieshout, J. J., Jenstrup, M., Pott, F. & Secher, N. H. (2003) Postural effects on cardiac output and mixed venous oxygen saturation in humans. *Exp. Physiol.*, **88**, 611–616.

van Heusden, K., Gislof, J., Stok, W. J., Dijkstra, S. & Karemaker, J. M. (2006) Mathematical modeling of gravitational effects on the circulation: importance of the time course of venous pooling and blood volume changes in the lungs. *Am. J. Physiol.*, **291**, H2152–H2165.

Huberts, W., Bode, A. S., Kroon, W., Planken, R. N., Tordoir, J. H. M. & van de Vosse, F. N. (2011) A pulse-wave propagation model to support decision-making in vascular access planning in the clinic. *Med. Eng. Phys.*, **34**, 233–248.

Ipsen, I. C. P., Kelley, C. T. & Pope, S. R. Rank-deficient nonlinear least squares problems and subset selection. *SIAM J. Numer. Anal.*, **49**, 1244–1266.

Kegler, C., Strunk, M. & Rudofsky, G. Venous pressure dynamics of the healthy human leg. *J. Vasc. Res.*, **38**, 20–29.

Kelley, C. T. (1999) *Iterative Methods for Optimization*. Philadelpha, PA: SIAM.

Lanier, J. B., Mote, M. B. & Clay, E. C. (2011) Evaluation and management of orthostatic hypotension. *Am. Fam. Physician*, **84**, 527–536.

Le Vey, G. & Vermeiren, C. (2000) Short term autonomic nervous control of the cardiovascular system: a system theoretic approach. *Mathematical Modeling in Medicine* (J. T. Ottesen & M. Danielasen eds). Amsterdam, The Netherlands: IOS Press.

van Lieshout, J. J, Harms, M. P. M., Pott, F., Jenstrup, M. & Secher, N. H. (2005) Stroke volume of the heart and thoracic fluid content during head up and head down tilt in humans. *Acta Anaesthesiol. Scand.*, **49**, 1287–1292.

Matzen, S., Perko, G., Groth, S., Friedman, D. B. & Secher, N. H. (1991) Blood volume distribution during head-up tilt induced central hypovolaemia in man. *Clin. Physiol.*, **11**, 411–422.

Melbin, J., Detweiler, D. K., Riffle, R. A. & Noordergraaf, A. (1982) Coherence of cardiac output with rate changes. *Am. J. Physiol.*, **243**, H499–H504.

Melchior, F. M., Srinivasen, R. S. & Charles, J. B. (1992) Mathematical modeling of human cardiovascular system for simulation of orthostatic response. *Am. J. Physiol.*, **262**, H1920–H1933.

Miller, T. H. & Kruse, J. E. (2005) Evaluation of syncope. *Am. Fam. Physician*, **72**, 1492–1500.

Møgelvang, J., Thomsen, C., Mehlsen, J., Brackle, M., Stubgaard, M. & Henriksen, O. (1986) Evaluation of left ventricular volumes measured by magnetic resonance imaging. *Eur Heart J.*, **7**, 1016–1021.

Ogoh, S., Brothers, R. M., Barnes, Q., Eubank, W. L., Hawkins, M. N., Purkayatha, S., O-Yurvati, A. & Raven, P. B. (2006) Effects of changes in central blood volume on carotid-vasomotor baroreflex sensitivity at rest and during exercise. *J. Appl. Physiol.*, **101**, 68–75.

Olansen, J. B., Clark, J. W., Khoury, D., Ghorbel, F. & Bidani, A. (2000) A closed-loop model of the canine cardiovascular system that includes ventricular interaction. *Comp. Biomed. Res.*, **33**, 260–295.

Olufsen, M. S., Alston, A., Tran, H. T., Ottesen, J. T. & Novak, V. (2008) Modeling heart rate regulation—Part I: sit-to-stand versus head-up tilt. *Cardiovasc. Eng.*, **8**, 73–87.

Olufsen, M. S., Nadim, A. & Lipsitz, L. A. (2002) Dynamics of cerebral blood flow regulation explained using a lumped parameter model. *Am. J. Physiol.*, **282**, R611–R622.

Olufsen, M. S. & Ottesen, J. T. (2012) A practical approach to parameter estimation applied to model predicting heart rate regulation. *J. Math. Biol.* doi:10.1007/s00285-012-0535-8.

Olufsen, M. S., Ottesen, J. T., Tran, H. T., Ellwein, L. M., Lipsitz, L. A. & Novak, V. (2005) Blood pressure and blood flow variation during postural change from sitting to standing: model development and validation. *J. Appl. Physiol.*, **99**, 1523–1537.

Olufsen, M. S., Tran, H. T., Ottesen, J. T., REU Program, Lipsitz, L. A. & Novak, V. (2006) Modeling baroreflex regulation of heart rate during orthostatic stress. *Am. J. Physiol.*, **291**, R1355–R1368.

Ottesen, J. T. (1997) Modeling of the baroreflex-feedback mechanism with time-delay. *J. Math. Biol.*, **36**, 41–63.

Ottesen, J. T. (2000) General compartmental models of the cardiovascular system. *Mathematical Modeling in Medicine* (J. T. Ottesen & M. Danielsen eds). Amsterdam, The Netherlands: IOS Press.

Ottesen, J. T. & Danielsen, M. (2009) Modeling ventricular contraction with heart rate changes. *J. Theor. Biol.*, **222**, 337–346.

Pope, S. R., Ellwein, L. M., Zapata, C. L., Novak, V., Kelly, C. T. & Olufsen, M. S. (2009) Estimation and identification of parameters in a lumped cerebrovascular model. *Math. Biosci. Eng.*, **6**, 93–115.

Porta, A., Bassani, T., Bari, V., Tobaldini, E., Takahashi, A. C., Catal, A. M. & Montano, N. (2011) Model-based assessment of baroreflex and cardiopulmonary couplings during graded head-up tilt. *Comput. Biol. Med.*, **42**, 298–305.

Rideout, V. C. (1991) *Mathematical and Computer Modeling of Physiological Systems*. Englewood Cliffs, NJ: Prentice Hall.

Robertson, D. W., Low, P. A. & Polinsky, R. J. (2004) *Primer on the Autonomic Nervous System*. San Diego, CA: Academic Press.

Rowell, L. B. (2004) Ideas about control of skeletal and cardiac muscle blood flow (1876–2003): cycles of revision and new vision. *J. Appl. Physiol.*, **97**, 384–392.

Segers, P., Qasem, A., de Backer, T., Carlier, S., Verdonck, P. & Avolio, A. (2001) Peripheral 'oscillatory' compliance is associated with aortic augmentation index. *Hypertension*, **37**, 1434–1439.

Seidel, H., Herzel, H. & Eckberg, D.L. (2004) Phase dependencies of the human baroreceptor reflex. *Am. J. Physiol.*, **272**, H2040–H2053.

Sheffer, L., Santamore, W. P. & Barnea, O. (2007) Cardiovascular simulation toolbox. *Cardiovsc. Eng.*, **7**, 81–88.

Shoemaker, W. (1989) Fluids and electrolytes in the acutely ill adult. *Textbook of Critical Care* (W. Shoemaker, S. Ayres, A. Grenvik, P. Holbrook & W. Leigh Thompson eds). Phiiladelphia, PA: W.B. Saunders.

Silvani, A., Magosso, E., Bastianini, S., Lenzl, P. & Ursino, M. (2011) Mathematical modeling of cardiovascular coupling: central autonomic commands and baroreflex control. *Auton. Neurosci.*, **162**, 66–71.

Smith, J. J. & Ebert, J. (1990) *General Response to Orthostatic Stress*. Boca Raton, FL: CRC Press.

Sprangers, R. L., Wesseling, K. H., Imholz, A. L. & Wieling, W. (1991) Initial blood pressure fall on stand up and exercise explained by changes in total peripheral resistance. *J. Appl. Physiol.*, **70**, 523–530.

Sun, J. X., Reisner, A. T., Saeed, M., Heldt, T. & Mark, R. G. (2009) The cardiac output from blood pressure algorithms trial. *Crit. Care Med.*, **37**, 72–80.

TenVoorde, B. J. & Kingma, R. (2000) A baroreflex model of short term blood pressure and heart rate variability. *Mathematical Modeling in Medicine* (J. T. Ottesen & M. Danielsen eds). Amsterdam, The Netherlands: IOS Press.

Tortora, G. J. & Anagnostakos, N. P. (1990) *Principles of Anatomy and Physiology*. New York, NY: Harper & Row, Publishers.

Triedman, J. K. & Saul, J. P. (1998) Blood pressure modulation by central venous pressure and respiration. Buffering effects of the heart rate reflexes. *Circulation*, **89**, 169–179.

Ursino, M. (1998) Interaction between carotid baroregulation and the pulsating heart: a mathematical model. *Am. J. Physiol.*, **275**, H1733–H1747.

Ursino, M. (1999) A mathematical model of the carotid baroregulation in pulsating conditions. *IEEE Trans. Biomed. Eng.*, **46**, 382–392.

van de Vooren, H., Gademan, M. G. J., Swenne, C. A., TenVoorde, B. J., Schalij, M. J. & Van der Wall, E. E. (2007) Baroreflex sensitivity, blood pressure buffering, and resonance: what are the links? Computer simulation of healthy subjects and heart failure patients. *J. Appl. Physiol.*, **102**, 1348–1356.

Wieling, W., Harms, M. P., ten Harkel, A. D., Lieshout, J. J. & Sprangers, R. L. (1996) Circulatory response evoked by a 3 s bout of dynamic leg exercise in humans. *J. Physiol.*, **494**, 601–611.

Zenker, S., Rubin, J. & Clermont, G. (2007) From inverse problems in mathematical physiology to quantitative differential diagnoses. *PloS Comp. Biol.*, **3**, 2072–2086.